nature physics

Article

https://doi.org/10.1038/s41567-024-02611-z

Emergence of fluctuating hydrodynamics in chaotic quantum systems

Received: 3 November 2023

Accepted: 9 July 2024

Published online: 12 August 2024

Check for updates

Julian F. Wienand[1,2,3] ✉, Simon Karch[1,2,3], Alexander Impertro[1,2,3], Christian Schweizer[1,2,3], Ewan McCulloch[4], Romain Vasseur[4], Sarang Gopalakrishnan[5], Monika Aidelsburger[1,2,3] & Immanuel Bloch[1,2,3] ✉

A fundamental principle of chaotic quantum dynamics is that local subsystems eventually approach a thermal equilibrium state. The corresponding timescales increase with subsystem size as equilibration is limited by the hydrodynamic build-up of fluctuations on extended length scales. We perform large-scale quantum simulations that monitor particle-number fluctuations in tunable ladders of hard-core bosons and explore how the build-up of fluctuations changes as the system crosses over from integrable to fully chaotic dynamics. Our results indicate that the growth of large-scale fluctuations in chaotic, far-from-equilibrium systems is quantitatively determined by equilibrium transport coefficients, in agreement with the predictions of fluctuating hydrodynamics. This emergent hydrodynamic behaviour of subsystem fluctuations provides a test of fluctuation–dissipation relations far from equilibrium and allows the accurate determination of equilibrium transport coefficients using far-from-equilibrium quantum dynamics.

Many-body quantum dynamics is intractable, in general. However, in chaotic quantum systems, the expectation values of local observables evolve simply[1,2]. Starting from a general initial state, these observables rapidly reach local equilibrium values corresponding to spatially varying temperatures and chemical potentials[3–5]. On longer timescales, these spatial variations relax through hydrodynamic processes such as diffusion[6,7]. It might seem that initial states without large-scale density variations (for example, translation-invariant initial product states) will, thus, rapidly relax. However, even such states exhibit slow timescales. The equilibrium state has much larger density fluctuations and entanglement than the initial state, and these quantities can only be built up by slow hydrodynamic processes[8] (Fig. 1). The equilibration of fluctuations goes beyond standard thermalization, as it involves highly non-local observables.

In the simpler setting of classical stochastic systems, the equilibration of fluctuations was only recently understood using fluctuating hydrodynamics (FHD), in which noise is explicitly added to the hydrodynamic equations[7,9]. A striking prediction of FHD is that the thermalization of large-scale fluctuations in generic far-from-equilibrium states is completely determined by equilibrium transport coefficients, such as the density- and temperature-dependent diffusion constant. This implies that a very strong form of the fluctuation–dissipation theorem emerges, even far from equilibrium, as a consequence of local thermalization. However, whether this prediction is borne out, and indeed whether the framework of FHD can even be applied in isolated quantum systems, remains an open question.

Experimentally, neutral atoms in optical lattices provide a compelling platform for studying the relaxation of many-body quantum systems and have been used to shed light on thermalization[10–13], many-body localization[14–19], quantum scarring[20], Hilbert space fragmentation[21,22], energy and correlation spreading[23,24], as well as diffusive transport[25–27]. In most cases, transport has been probed through the dynamics of local expectation values in non-equilibrium states[10]. The invention of quantum-gas microscopy[28–30] has made subsystem

[1]Fakultät für Physik, Ludwig-Maximilians-Universität, Munich, Germany. [2]Max-Planck-Institut für Quantenoptik, Garching, Germany. [3]Munich Center for Quantum Science and Technology (MCQST), Munich, Germany. [4]Department of Physics, University of Massachusetts, Amherst, MA, USA. [5]Department of Electrical and Computer Engineering, Princeton University, Princeton, NJ, USA. ✉e-mail: j.wienand@lmu.de; immanuel.bloch@mpq.mpg.de

https://doi.org/10.1038/s41567-024-02611-z

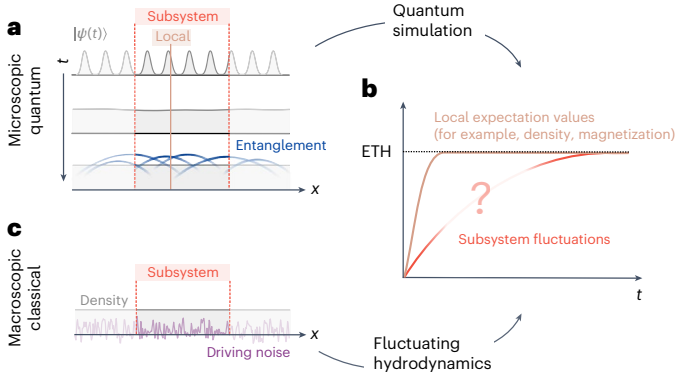

Fig. 1 | Emergence of hydrodynamic fluctuations in a chaotic quantum system. a, In an out-of-equilibrium quantum system without large-scale density variations, local expectation values (such as density) rapidly relax, while entanglement keeps spreading across the system on much longer timescales. **b**, Thus, a subsystem becomes increasingly entangled with its environment, leading to fluctuations of observables in the subsystem that equilibrate on a much slower timescale than local expectation values. Eventually, thermal equilibrium is reached, as described by the eigenstate thermalization hypothesis (ETH). **c**, This slow hydrodynamic equilibration of fluctuations is conjectured to be classically described by FHD, which predicts the time evolution of the statistics of a coarse-grained density $n(x, t)$ driven by statistical noise.

correlations and entanglement[11,16,17,31,32] detectable in experiments. Such studies have either been limited to small systems or not probed the time evolution of correlations. However, observing slow hydrodynamic timescales relevant to the build-up of fluctuations on large length scales requires both large systems and the ability to track the dynamical evolution of fluctuations while avoiding any boundary effects.

In this work, we investigate the equilibration of fluctuations in large quantum systems using a ^{133}Cs quantum-gas microscope[33,34]. The atoms were arranged in a large ladder geometry containing up to 100 sites, with adjustable rung couplings, which allowed us to tune the dynamics from integrable to fully chaotic. The interactions were set to the regime of hard-core bosons using an external magnetic field and a Feshbach resonance. To characterize the build-up of fluctuations, we measured the particle number inside subsystems of various size after a quantum quench and studied the time evolution of its variance (Fig. 2c). We showed that, in the chaotic case, the rate of growth of density fluctuations appeared to be completely determined by the equilibrium transport properties of the system and could be quantitatively described by FHD. We provide a heuristic argument for how this result arises in an isolated quantum system by appealing to an emergent hydrodynamic description of quantum operator evolution in which long, complex operators act as a noisy bath driving fluctuations of simple hydrodynamic degrees of freedom[8]. In this picture, equal-time correlation functions, and therefore particle-number fluctuations following a quantum quench, are intimately related to the equilibrium linear response. We compared these predictions with experimental results for the chaotic ladder and found excellent quantitative agreement. This agreement is a stringent test of the fluctuation–dissipation relations outside equilibrium[9]. It allows for a precise determination of the linear-response diffusion constants from quantum simulations of far-from-equilibrium dynamics and demonstrates the capability of quantum simulators to compute quantities that are difficult to obtain using numerical methods[8,35].

Furthermore, as we tuned the dynamics from integrable to chaotic, we observed that the local mean densities relaxed increasingly fast, whereas the growth of large-scale fluctuations was slowed down. This clear separation of equilibration timescales highlights the distinction between the relaxation of local expectation values (mean density) and that of non-local quantities (large-scale fluctuations). Our work provides a direct observation of the crossover from ballistic to diffusive correlation growth in an isolated quantum system.

Experimental protocol

In our experiments, we used a strongly interacting quantum gas of ^{133}Cs atoms imaged using a quantum-gas microscopy set-up with a high numerical aperture. After preparing a Bose–Einstein condensate in a single plane of a vertical optical lattice at the focus of the objective, the atoms were loaded into a two-dimensional superlattice potential, consisting of an optical superlattice in the y direction ($\lambda_{y,\mathrm{short}} = 767$ nm and $\lambda_{y,\mathrm{long}} = 1{,}534$ nm) and a simple lattice in the x direction ($\lambda_{x,\mathrm{short}} = 767$ nm). The resulting potential is characterized by chains of double wells coupled in the y direction (Fig. 2) and enables us to realize the Bose–Hubbard model in ladder geometries, as expressed by the Hamiltonian:

$$\hat{H} = -J\left(\sum_{\alpha,i} \hat{a}^{\dagger}_{\alpha,i}\hat{a}_{\alpha,i+1} + \text{h.c.}\right) - J_{\perp}\left(\sum_{i} \hat{a}^{\dagger}_{1,i}\hat{a}_{2,i} + \text{h.c.}\right) + \frac{U}{2}\sum_{\alpha,i} \hat{n}_{\alpha,i}(\hat{n}_{\alpha,i} + 1). \quad (1)$$

Here, $\hat{a}_{\alpha,i}$, $\hat{a}^{\dagger}_{\alpha,i}$ and $\hat{n}_i = \hat{a}^{\dagger}_{\alpha,i}\hat{a}_{\alpha,i}$ are the bosonic annihilation, creation and particle-number operators for site i in leg $\alpha = 1, 2$ of the ladder[36,37]. Atoms can tunnel along (perpendicular to) the ladder with strength J ($J_{\perp}$). The on-site interaction energy is denoted by U. All measurements were performed in the hard-core regime with $U/J > 7$ (see Supplementary Information Section IC for details). In the experiment, there were 20 identical uncoupled ladders (Fig. 2a), each of which contained up to 2×50 sites. The harmonic confinement of the vertical lattice was compensated for by a tailored light profile shaped using a digital mirror device to realize a homogeneous box potential with hard walls marking the two ends of the ladder systems.

We began an experiment by preparing a period-two CDW (charge density wave), as shown in Fig. 2a, using an extra optical superlattice potential in the x direction ($\lambda_{x,\mathrm{short}} = 767$ nm and $\lambda_{x,\mathrm{long}} = 1{,}534$ nm). This initial CDW was close to a product state in which every other site along the ladder was occupied by one atom, as shown in Fig. 2a (refs. 10,12,14,18,38–40). Typically, we achieved a filling of 84(8)% in the occupied and 4(3)% in the unoccupied rows. Importantly, the CDW was spatially uniform on large scales but displayed strongly suppressed particle-number fluctuations compared to an equilibrium state.

First, the entire dynamics was frozen, so that $J_{\perp} \approx J \approx 0$. We then quenched on the tunnel coupling to $J/h = 96(3)$ Hz with $J_{\perp}/J \approx 0$, $J_{\perp}/J = 0.55(2)$ or $J_{\perp}/J = 1.04(3)$, where h is the Planck constant. We set the coupling between the legs of the ladder and let the system evolve for a controllable evolution time t (see Supplementary Information Section I for more details of the experimental set-up and sequence). Tuning the tunnelling rate between the two legs of each ladder allowed us to interpolate between a regime of decoupled chains and one in which the bosons on the two legs were strongly interacting. The decoupled regime was integrable[41] and mapped to free fermions with infinitely many conserved quantities, namely the occupation numbers of each single-particle eigenstate. By contrast, the fully coupled regime was strongly chaotic, so that all local observables relaxed rapidly except for the energy and particle-number densities.

Local mean density decay

As the initial (perfect) CDW state lacked large-scale density gradients, hydrodynamics predicts that local expectation values—the simplest observables—should rapidly relax. For this initial state, a natural expectation value is the average imbalance $\mathcal{I} = (\langle\hat{n}_{\mathrm{even}}\rangle - \langle\hat{n}_{\mathrm{odd}}\rangle) / (\langle\hat{n}_{\mathrm{even}}\rangle + \langle\hat{n}_{\mathrm{odd}}\rangle)$ of all ladder systems in the region of interest of 40×40 sites. It compares the average filling of even $\langle\hat{n}_{\mathrm{even}}\rangle = \langle\hat{n}_{2i}\rangle_i$ and odd

https://doi.org/10.1038/s41567-024-02611-z

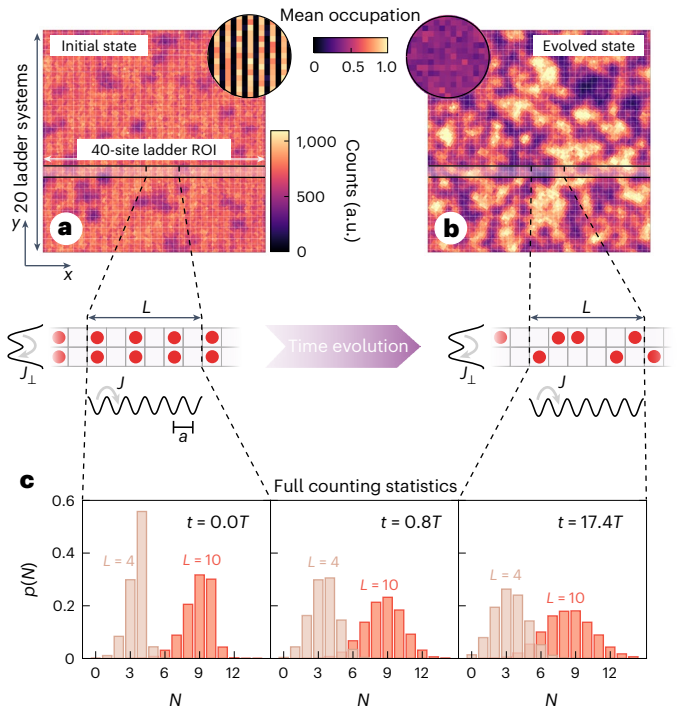

Fig. 2 | Equilibration in ladder systems with tunable rung coupling. **a**,**b**, Several copies of large homogeneous ladder systems are realized using an optical superlattice in the *y* direction and a simple lattice in the *x* direction. Each 1D chain has a length of up to 50 sites (delimited by potential walls created using a digital mirror device), the central 40 of which are in the region of interest used for data analysis. Adjusting $J_\perp/J$ allows us to smoothly tune between integrable uncoupled 1D systems of hard-core bosons ($J_\perp/J = 0$) and fully coupled ladder systems ($J_\perp/J = 1$) with chaotic dynamics. **a**, The initial state is a CDW with a period of two lattice constants. It is prepared using an optical superlattice in the *x* direction. Inset, reconstructed site occupation averaged over 32 images. **b**, After quenching the system to large tunnel couplings, the CDW rapidly evolves into a state with uniform filling and slowly growing subsystem fluctuations. **c**, Using single-site resolution, we obtained the full counting statistics $p(N)$ of the total particle number N in subsystems of length L with $2L$ sites (here shown for two subsystem sizes $L = 4$ and 10 and three different evolution times t in units of tunnelling time $T = \hbar/J$) and use it to track the relaxation dynamics after the quench.

sites $\langle \hat{n}_{\mathrm{odd}} \rangle = \langle \hat{n}_{2i+1} \rangle_i$ (refs. 10,14). As shown in Fig. 3a, the imbalance decayed to zero on timescales comparable to the tunnelling strength J for all $J_\perp/J$. We extracted the decay constant τ by fitting an exponentially decaying Bessel function $\mathcal{I}(t) = A\mathcal{J}_0(4t/T)\,\mathrm{e}^{-t/\tau}$ with amplitude A (ref. 42).

To motivate this fit, note that in the one-dimensional (1D) case ($J_\perp/J = 0$), the dynamics can be mapped onto that of free fermions through a Jordan–Wigner transformation. Free-fermion theory predicts a purely Bessel-type decay with $\tau \to \infty$ and $A = 1$. However, due to the imperfect filling of the initial state with $\mathcal{I}(0) \approx 0.9$, the fitted amplitude reduced to $A = 0.9$ (dashed curve in Fig. 3a). Furthermore, the finite decay constant measured even for $J_\perp/J = 0$ can most probably be attributed to disorder with an amplitude on the order of J (Supplementary Information Section III). We found that the decay of the oscillation was enhanced for larger $J_\perp/J$. This was due to the integrability-breaking interactions between adjacent chains, which dephased the oscillations that occurred in the free-fermion limit and entailed a faster decay of the imbalance.

Number fluctuations

Although the density reached equilibrium rapidly, subsystem number fluctuations showed a strikingly different behaviour. We quantify fluctuations through the variance of the particle number inside a ladder region of length L with $2L$ sites, $\mathrm{Var}_L \equiv \mathrm{Var}\left(\sum_i^L \hat{N}_i\right)$, where $\hat{N}_i = \hat{n}_{1,i} + \hat{n}_{2,i}$ is the total particle number in the ith rung of the ladder. This quantity is computed from density–density correlators (see below) to mitigate systematic reconstruction errors. As explained in Supplementary Information Section II, we applied a calibrated short-distance correction to the density–density correlation data, which was then used to compute the particle-number fluctuations.

In the perfect CDW state, the variance is zero, but as the subsystem interacts (and becomes entangled) with its surroundings, this variance eventually builds up to its thermal equilibrium value, which is expected to be close to the value at infinite temperature $2L\bar{n}(1-\bar{n})$ for an infinite disorder-free system in the hard-core regime ($\bar{n}$ is the average filling). The equilibrium fluctuations are expected to emerge on timescales that are ballistic in the integrable limit and diffusive in the chaotic limit. Thus, chaotic dynamics slows down the relaxation of non-local quantities, including atom-number fluctuations. Figure 3b depicts the time evolution of the normalized variance $\overline{\mathrm{Var}}_L(t) = [\mathrm{Var}_L(t) - \mathrm{Var}_L(0)]/[\mathrm{Var}_L(\infty) - \mathrm{Var}_L(0)]$ for various system sizes L and $J_\perp/J \approx 0.0$, 0.5 and 1.0. Here, $\mathrm{Var}_L(\infty)$ is the saturation value for $t \to \infty$, which is extracted from a fitting procedure that uses an empirical function (Supplementary Information Section IIF). To quantify the rate of growth of fluctuations, we define the saturation time t_{sat} at which the variance reaches 80% of its long-time saturation value.

We found that larger subsystems exhibit a variance growth that is substantially slower in the ladder ($J_\perp/J \approx 1.0$) compared to the 1D case ($J_\perp/J \approx 0.0$). This is visualized by the data points in Fig. 3b, which show t_{sat} as a function of the size of the subsystem L. In Fig. 3c, the same data are shown with log–log scaling, which reveals that the saturation time t_{sat} scales polynomially with subsystem size L, so that $L \propto t_{\mathrm{sat}}^{1/z}$ with scaling exponent z. Using a linear fit to extract the slope, we found $z = 1.07(6)$, 1.4(2) and 2.2(4) for $J_\perp/J \approx 0.0$, 0.5 and 1.0, respectively. This is consistent with the expectation that the dynamics in the decoupled chains ($J_\perp/J = 0.0$) is ballistic ($z = 1$) and the dynamics in the system with fully coupled legs ($J_\perp/J = 1.0$) is diffusive ($z = 2$). For $J_\perp/J = 0.5$, we found an intermediate value that can be interpreted as a crossover from integrable to chaotic dynamics with diffusive behaviour at long times. We also observed that large-scale fluctuations failed to fully thermalize (Supplementary Information Section IIIC).

Figure 4 compares the fitted equilibration timescales of the mean density (τ in Fig. 3a) and the particle-number fluctuations (t_{sat} in Fig. 3c), It reveals a separation of equilibration timescales, which became increasingly pronounced as the coupling within the ladder was increased. This shows that even when the expectation values relax rapidly, large-scale fluctuations can exhibit much slower (hydrodynamic) timescales.

Density–density correlations

Using our quantum-gas microscope, we measured the rung-density correlation function $C_{\mathrm{d}} = \langle \hat{N}_i \hat{N}_j \rangle - \langle \hat{N}_i \rangle \langle \hat{N}_j \rangle$ over distances up to $|d| = 21$, where $d = i - j$ denotes the real-space distance between two sites with indices i and j. The particle-number variance studied previously combines these correlations into a single quantity. We used spatially resolved correlations to shed further light on the dynamics that govern the thermalization process as we crossed from integrable ($J_\perp/J \approx 0$) to chaotic dynamics ($J_\perp/J > 0$).

Figure 5a shows C_{d} as a function of distance and evolution time. It reveals a cone that illustrates how the correlations emerge after the quench and how they grow spatially during equilibration[23,24,43]. The slope of the cone boundary indicates the maximum speed of correlation spreading. For the 1D integrable system ($J_\perp/J \approx 0.0$), the boundary of the cone is linear with a slope consistent with $4Ja/\hbar$ (dashed line), where $a = 383.5$ nm is the lattice spacing. This suggests the ballistic spreading at the Lieb–Robinson velocity predicted by free-fermion theory[23,44]. For $J_\perp/J > 0$, the onset of the cone at short times is characterized by the

https://doi.org/10.1038/s41567-024-02611-z

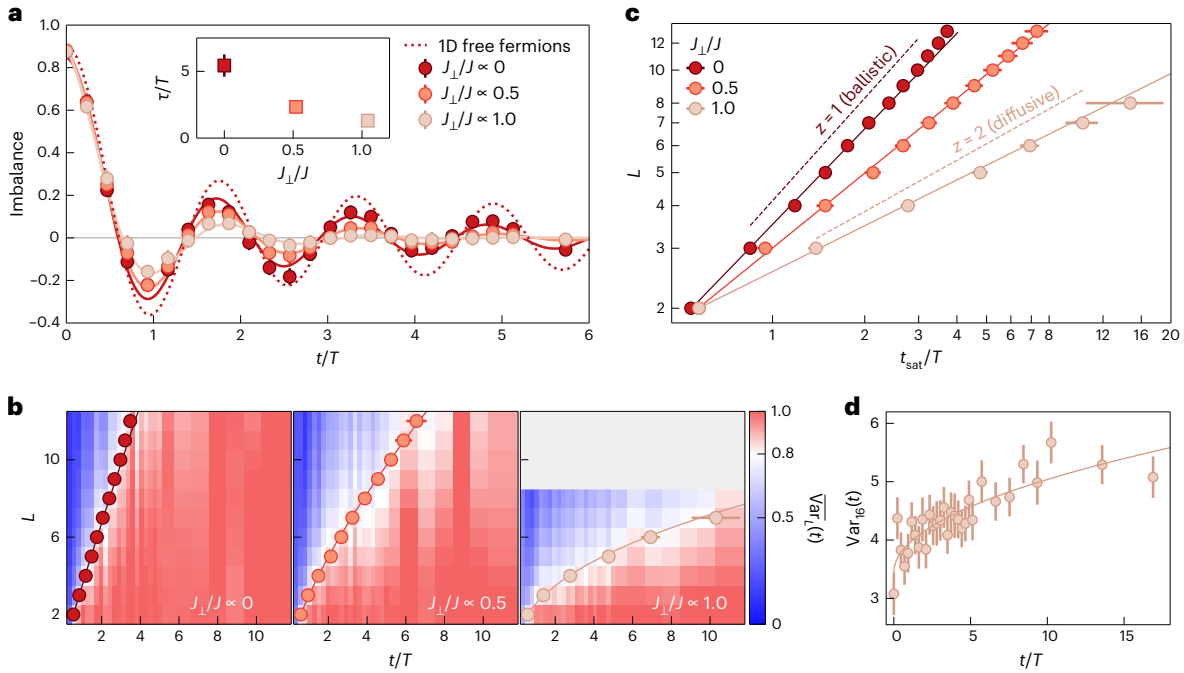

Fig. 3 | Time evolution of the local mean density and particle-number fluctuations. a, Imbalance as a function of evolution time for $J_\perp/J \approx 0.0$, 0.5 and 1.0. Each data point was obtained from averaging over the region of interest with 40 × 40 sites and about 35 fluorescence images. Solid curves are Bessel function fits to the experimental data (see text for details). The dotted curve is the theoretical expectation for the 1D chain, which was derived from free-fermion theory and takes into account the imperfect initial experimental state. Inset, Fitted 1/e decay constant τ as a function of $J_\perp/J$. Error bars denote the standard deviation. **b**, Normalized atom-number variances $\overline{\mathrm{Var}_L}(t)$ in ladder subsystems of size $2L$. The data points indicate the time t_{sat} when the variance reached 80% of its fitted saturation value. The grey area in the right-hand panel marks the regime of very large subsystems for which we could not reliably determine the saturation value as the fluctuation growth was too slow. The error bars indicate the standard error of the fit used to determine t_{sat}. The solid lines are the same fits as in **c**. **c**, Threshold time t_{sat} as a function of subsystem size L and $J_\perp/J$ in log–log scale. The solid lines are linear fits used to obtain the dynamical exponent $L \propto t_{\mathrm{sat}}^{1/z}$. For reference, the dashed lines indicate ideal slopes corresponding to $z = 1$ or 2 for ballistic and diffusive dynamics. **d**, Atom-number variance for a subsystem of size $L = 16$ as a function of evolution time. The solid line is the FHD prediction fitted to the experimental data, which yields a diffusion constant $D = 1.11(25)\,Ja^2/\hbar$, where a denotes the lattice spacing. Error bars denote the standard deviation.

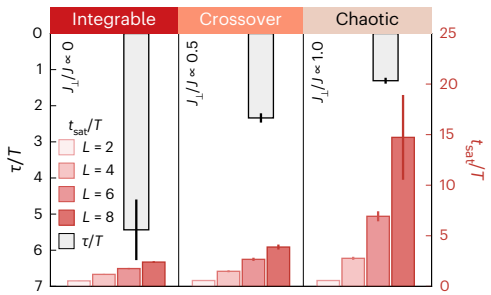

Fig. 4 | Separation of equilibration timescales. Imbalance decay constant τ (Fig. 3a) and the variance growth threshold time t_{sat} for various subsystem sizes (Fig. 5b,c) as a function of $J_\perp/J$, showing opposite behaviour in the limits $J_\perp/J \approx 0.0$ and 1.0. Error bars denote the standard error. Although local expectation values relax faster in the chaotic limit, the subsystem fluctuation growth slows down, creating a separation of equilibration timescales between different moments of the particle-number distribution.

same slope. However, at later times, the cone's expansion slows down according to a square-root law, indicating that the correlations eventually spread in a diffusive fashion.

Hydrodynamics of fluctuations

We have presented evidence that fluctuations starting from a non-equilibrium initial state (in the chaotic ladder) grow diffusively. We now turn to a remarkable quantitative FHD prediction about this diffusive growth, namely, that the diffusion constant observed in this far-from-equilibrium setting should precisely match the near-equilibrium, linear-response diffusion constant at the temperature and density set by the initial state $|\psi_0\rangle$ (in this case, infinite temperature and half filling). This claim can be equivalently expressed as a conjecture relating the late-time behaviour of two distinct correlation functions: $\langle\psi_0|\hat{n}(x,t)\hat{n}(0,t)|\psi_0\rangle$ —which we can measure experimentally—and $\mathrm{Tr}(\hat{n}(x,t)\hat{n}(0,0))$—which sets the linear-response conductivity. Note that these correlation functions are mathematically rather different; the conjecture relating them is much stronger than, for example, the eigenstate thermalization hypothesis[3,4], which is concerned only with whether local expectation values eventually relax to their thermal equilibrium values.

We now briefly sketch the argument leading to this conjecture. A detailed derivation and further supporting numerical evidence are presented in Supplementary Information Section IV. We begin by considering the Heisenberg-evolved operator $\hat{n}_i(t)$. Due to atom-number conservation, one can write $\hat{n}_i(t) = \sum_j c_j \hat{n}_j(t) + \ldots$, where $\sum_j c_j = 1$. The terms in … correspond to multisite operators encoding the high-order correlations that are generated under chaotic dynamics. A widely accepted conjecture is that these complicated operators do not contribute to few-point correlators[8]. Mathematically, neglecting these complicated operators is like introducing dephasing noise, which would explicitly suppress them. This hydrodynamic assumption then reduces the dynamics of the quantum density correlators to the correlators under the classical noisy diffusion equation:

$$\partial_t n + \partial_x j = 0, \quad j = -D\,\partial_x n + \sqrt{2D\chi(n)}\,\xi, \tag{2}$$

where j is the particle current, $\chi(n) = n(1-n)$ is the static susceptibility and $\xi(x,t)$ is a Gaussian white noise process with unit variance

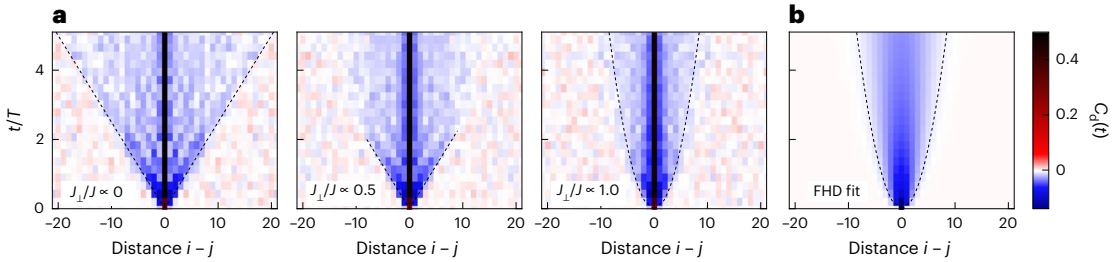

Fig. 5 | Time evolution of two-point rung-density correlations. a, Rung-density–density correlations $C_d(t)$ showing a cone that indicates ballistic spreading for $J_\perp/J \approx 0.0$ and diffusive spreading for $J_\perp/J \approx 1.0$. The dashed lines in the left-hand and centre panels indicate the Lieb–Robinson velocity $4Ja/\hbar$ in the ballistic regime[44]. The correlations at each point in time were obtained from ≈35 fluorescence images. **b**, Gaussian fit for the density–density correlations predicted by FHD (see equation (9) in the Supplementary Information), fitted for $J_\perp/J \approx 1.0$ and distances $1 \le d \le 20$, which yielded a diffusion constant $D = 1.11(25)Ja^2/\hbar$. The dashed curves in **a** (right-hand panel) and **b** indicate the $2\sigma_c$ envelope of the Gaussian fit function, where $\sigma_c = \sqrt{4Dt/a^2}$.

(Supplementary Information Section IV). Under this assumption, the conjecture relating linear-response diffusion and the growth of fluctuations can readily be established. One can understand the emergence of noise from entanglement as follows. Each region of the system becomes strongly entangled with the rest of the system. Thus, to get a local description of the region, one has to fix the state of the rest of the system, which leads to projection noise.

In Supplementary Information Section IV we show that the growth of the variance of the particle number in a subsystem of length L is given by:

$$\mathrm{Var}_L^{\mathrm{CDW}}(t) \approx \sqrt{\frac{2Dt}{\pi a^2}}, \quad t \ll (La)^2/D, \tag{3}$$

starting from a perfect CDW state, before its eventual equilibration at times ~$(La)^2/D$. This enables us to determine the diffusion constant from the particle-number fluctuations in large subsystems with far-from-equilibrium fluctuations. Using the $L = 16$ data shown in Fig. 3d, we find $D = 1.11(25)Ja^2/\hbar$.

Alternatively, we can also obtain the diffusion constant by fitting the correlation cone in Fig. 5a (right-hand panel) for $J_\perp/J \approx 1.0$, which we expect to spread as a Gaussian with width $\sqrt{4Dt/a^2}$ (Supplementary Information Section IIE). This yields $D = 0.88(5)Ja^2/\hbar$ (Fig. 5b), which is in good agreement with the value obtained from particle-number fluctuations. Importantly, both experimental values for the diffusion coefficient match estimates from recent theoretical equilibrium linear-response predictions[35,45], suggesting that FHD provides not only a qualitative but also a quantitative description of the post-quench dynamics of isolated quantum systems. By extracting the diffusion constant from the correlation cone, we build a bridge between equal-time correlation functions following a quench from a far-from-equilibrium initial state and two-time correlation functions about an equilibrium initial state. The former manifest themselves as number fluctuations that grow from the initial CDW state, whereas the latter characterize linear-response coefficients, including the diffusion constant, which uniquely defines the entire macroscopic time evolution of charge fluctuations.

Discussion

Most studies of thermalization in isolated quantum systems have focused on local mean values, such as the average density or the imbalance. By studying the equilibration dynamics of non-local quantities, such as particle-number fluctuations and density–density correlators, we have identified a crossover from integrable (ballistic) to chaotic (diffusive) dynamics. The measured diffusion constant extracted from non-equilibrium fluctuations agrees quantitatively with theoretical equilibrium linear-response predictions. This agreement provides suggestive evidence that FHD quantitatively describes the large-scale density fluctuations in many-body quantum systems.

As FHD relates the linear-response behaviour (which is hard to measure or compute) to fluctuation growth (which is straightforward to measure), our findings pave the way for a new class of experimental studies in which transport is characterized through fluctuation growth. Compared with protocols such as quenches from a domain-wall initial state[15,46] that involve the dynamics of local expectation values, using a CDW as an initial state has a strong advantage. The CDW rapidly approaches a local equilibrium state with uniform average density. Thus, quenches from a CDW allow one to directly probe equilibrium transport quantities while working far from a linear-response limit and retaining a high signal-to-noise ratio.

Natural targets for future exploration include a variety of many-body systems that lie at or beyond the edge of current computational capabilities, including those with finite interactions beyond the hard-core approximation. Our large system with ≈2,500 sites could particularly benefit detailed studies of pre-thermalization[18,47,48] and many-body localization[16,19,49] in one and two dimensions. The ability to prepare a wide variety of initial states could facilitate quantum simulations of Hilbert space fragmentation and many-body scars[20–22,50] under the microscope to shed light on systems with exotic thermalization properties.

Although our results only systematically address the first two moments of physical observables, a natural question is whether each higher moment of these observables relaxes on a separate timescale. In addition to the duration of these relaxation processes, it is not well understood under what conditions these processes can reach infinite-temperature saturation values in finite systems and to what extent thermalization fails.

Online content

Any methods, additional references, Nature Portfolio reporting summaries, source data, extended data, supplementary information, acknowledgements, peer review information; details of author contributions and competing interests; and statements of data and code availability are available at https://doi.org/10.1038/s41567-024-02611-z.

References

1. Nandkishore, R. & Huse, D. A. Many-body localization and thermalization in quantum statistical mechanics. *Annu. Rev. Condens. Matter Phys.* **6**, 15–38 (2015).
2. D'Alessio, L., Kafri, Y., Polkovnikov, A. & Rigol, M. From quantum chaos and eigenstate thermalization to statistical mechanics and thermodynamics. *Adv. Phys.* **65**, 239–362 (2016).
3. Deutsch, J. M. Quantum statistical mechanics in a closed system. *Phys. Rev. A* **43**, 2046–2049 (1991).
4. Srednicki, M. Chaos and quantum thermalization. *Phys. Rev. E* **50**, 888–901 (1994).
5. Rigol, M., Dunjko, V. & Olshanii, M. Thermalization and its mechanism for generic isolated quantum systems. *Nature* **452**, 854–858 (2008).

6. Lux, J., Müller, J., Mitra, A. & Rosch, A. Hydrodynamic long-time tails after a quantum quench. *Phys. Rev. A* **89**, 053608 (2014).
7. Spohn, H. *Large Scale Dynamics of Interacting Particles* (Springer, 1991).
8. von Keyserlingk, C., Pollmann, F. & Rakovszky, T. Operator backflow and the classical simulation of quantum transport. *Phys. Rev. B* **105**, 245101 (2022).
9. Bertini, L., De Sole, A., Gabrielli, D., Jona-Lasinio, G. & Landim, C. Macroscopic fluctuation theory. *Rev. Mod. Phys.* **87**, 593–636 (2015).
10. Trotzky, S. et al. Probing the relaxation towards equilibrium in an isolated strongly correlated one-dimensional Bose gas. *Nat. Phys.* **8**, 325–330 (2012).
11. Kaufman, A. M. et al. Quantum thermalization through entanglement in an isolated many-body system. *Science* **353**, 794–800 (2016).
12. Zhou, Z.-Y. et al. Thermalization dynamics of a gauge theory on a quantum simulator. *Science* **377**, 311–314 (2022).
13. Erne, S., Bücker, R., Gasenzer, T., Berges, J. & Schmiedmayer, J. Universal dynamics in an isolated one-dimensional Bose gas far from equilibrium. *Nature* **563**, 225–229 (2018).
14. Schreiber, M. et al. Observation of many-body localization of interacting fermions in a quasirandom optical lattice. *Science* **349**, 842–845 (2015).
15. Choi, J.-Y. et al. Exploring the many-body localization transition in two dimensions. *Science* **352**, 1547–1552 (2016).
16. Rispoli, M. et al. Quantum critical behaviour at the many-body localization transition. *Nature* **573**, 385–389 (2019).
17. Lukin, A. et al. Probing entanglement in a many-body-localized system. *Science* **364**, 256–260 (2019).
18. Rubio-Abadal, A. et al. Many-body delocalization in the presence of a quantum bath. *Phys. Rev. X* **9**, 041014 (2019).
19. Léonard, J. et al. Probing the onset of quantum avalanches in a many-body localized system. *Nat. Phys.* **19**, 481–485 (2023).
20. Su, G.-X. et al. Observation of unconventional many-body scarring in a quantum simulator. *Phys. Rev. Res.* **5**, 023010 (2023).
21. Scherg, S. et al. Observing non-ergodicity due to kinetic constraints in tilted Fermi-Hubbard chains. *Nat. Commun.* **12**, 4490 (2021).
22. Kohlert, T. et al. Exploring the regime of fragmentation in strongly tilted Fermi–Hubbard chains. *Phys. Rev. Lett.* **130**, 010201 (2023).
23. Cheneau, M. et al. Light-cone-like spreading of correlations in a quantum many-body system. *Nature* **481**, 484–487 (2012).
24. Takasu, Y. et al. Energy redistribution and spatiotemporal evolution of correlations after a sudden quench of the Bose–Hubbard model. *Sci. Adv.* **6**, eaba9255 (2020).
25. Hild, S. et al. Far-from-equilibrium spin transport in Heisenberg quantum magnets. *Phys. Rev. Lett.* **113**, 147205 (2014).
26. Jepsen, N. et al. Spin transport in a tunable Heisenberg model realized with ultracold atoms. *Nature* **588**, 403–407 (2020).
27. Brown, P. T. et al. Bad metallic transport in a cold atom Fermi-Hubbard system. *Science* **363**, 379–382 (2019).
28. Bakr, W. S., Gillen, J. I., Peng, A., Fölling, S. & Greiner, M. A quantum gas microscope for detecting single atoms in a Hubbard-regime optical lattice. *Nature* **462**, 74–77 (2009).
29. Sherson, J. F. et al. Single-atom-resolved fluorescence imaging of an atomic Mott insulator. *Nature* **467**, 68–72 (2010).
30. Gross, C. & Bakr, W. S. Quantum gas microscopy for single atom and spin detection. *Nat. Phys.* **17**, 1316–1323 (2021).
31. Zhang, X., Kim, E., Mark, D. K., Choi, S. & Painter, O. A superconducting quantum simulator based on a photonic-bandgap metamaterial. *Science* **379**, 278–283 (2023).
32. Zheng, Y.-G. et al. Efficiently extracting multi-point correlations of a Floquet thermalized system. Preprint at https://arxiv.org/abs/2210.08556 (2022).
33. Klostermann, T. et al. Fast long-distance transport of cold cesium atoms. *Phys. Rev. A* **105**, 043319 (2022).
34. Impertro, A. et al. An unsupervised deep learning algorithm for single-site reconstruction in quantum gas microscopes. *Commun. Phys.* **6**, 166 (2023).
35. Rakovszky, T., von Keyserlingk, C. W. & Pollmann, F. Dissipation-assisted operator evolution method for capturing hydrodynamic transport. *Phys. Rev. B* **105**, 075131 (2022).
36. Crépin, F., Laflorencie, N., Roux, G. & Simon, P. Phase diagram of hard-core bosons on clean and disordered two-leg ladders: Mott insulator-Luttinger liquid-Bose glass. *Phys. Rev. B* **84**, 054517 (2011).
37. Donohue, P. & Giamarchi, T. Mott-superfluid transition in bosonic ladders. *Phys. Rev. B* **63**, 180508 (2001).
38. Lüschen, H. P. et al. Observation of slow dynamics near the many-body localization transition in one-dimensional quasiperiodic systems. *Phys. Rev. Lett.* **119**, 260401 (2017).
39. Kohlert, T. et al. Observation of many-body localization in a one-dimensional system with a single-particle mobility edge. *Phys. Rev. Lett.* **122**, 170403 (2019).
40. Yang, B. et al. Observation of gauge invariance in a 71-site Bose–Hubbard quantum simulator. *Nature* **587**, 392–396 (2020).
41. Kinoshita, T., Wenger, T. & Weiss, D. S. A quantum Newton's cradle. *Nature* **440**, 900–903 (2006).
42. Cramer, M., Flesch, A., McCulloch, I. P., Schollwöck, U. & Eisert, J. Exploring local quantum many-body relaxation by atoms in optical superlattices. *Phys. Rev. Lett.* **101**, 063001 (2008).
43. Tajik, M. et al. Experimental observation of curved light-cones in a quantum field simulator. *Proc. Natl Acad. Sci. USA* **120**, e2301287120 (2023).
44. Lieb, E. H. & Robinson, D. W. The finite group velocity of quantum spin systems. *Commun. Math. Phys.* **28**, 251–257 (1972).
45. Steinigeweg, R., Heidrich-Meisner, F., Gemmer, J., Michielsen, K. & De Raedt, H. Scaling of diffusion constants in the spin-1/2 XX ladder. *Phys. Rev. B* **90**, 094417 (2014).
46. Wei, D. et al. Quantum gas microscopy of Kardar–Parisi–Zhang superdiffusion. *Science* **376**, 716–720 (2022).
47. Gring, M. et al. Relaxation and prethermalization in an isolated quantum system. *Science* **337**, 1318–1322 (2012).
48. Ueda, M. Quantum equilibration, thermalization and prethermalization in ultracold atoms. *Nat. Rev. Phys.* **2**, 669–681 (2020).
49. Bordia, P. et al. Probing slow relaxation and many-body localization in two-dimensional quasi-periodic systems. *Phys. Rev. X* **7**, 041047 (2017).
50. Turner, C. J., Michailidis, A. A., Abanin, D. A., Serbyn, M. & Papic, Z. Quantum many-body scars. *Nat. Phys.* **14**, 745–749 (2018).

Data availability

The data that support the plots within this paper and other findings of this study are available at https://doi.org/10.17617/3.L50Q6I.

Code availability

The code used for data evaluation within this document is available from the corresponding author upon reasonable request.

Acknowledgements

We thank J. De Nardis, D. Huse, V. Khemani, A. Morningstar and B. H. Madhusudhana for helpful discussions. The work by the Munich team received funding from the German Research Foundation through Research Unit FOR5522 (Project No. 499180199) and under Germany's Excellence Strategy (Grant No. EXC-2111 - 390814868) and from the German Federal Ministry of Education and Research through the funding programme for quantum technologies from basic research to market (Contract No. 13N15895 FermiQP). J.F.W. acknowledges support from the German Academic Scholarship Foundation and the Marianne-Plehn-Program. S.K. receives funding from the International Max Planck Research School for Quantum Science and Technology. A.I. was supported by the Bavarian excellence network ENB through the International PhD Programme of Excellence Exploring Quantum Matter. C.S. has received funding from the European Union's Framework Programme for Research and Innovation Horizon 2020 (2014–2020) under a Marie Skłodowska-Curie Grant (Agreement No. 754388, LMUResearchFellows) and from LMUexcellent, which is funded by the Federal Ministry of Education and Research and the Free State of Bavaria under the Excellence Strategy of the German Federal Government and the Länder. Furthermore, we acknowledge support from the National Science Foundation (Grant Nos. DMR-2103938 to S.G. and E.M. and DMR-2104141 to E.M. and R.V.) and the Alfred P. Sloan Foundation through Sloan Research Fellowships (R.V.).

Author contributions

J.F.W., S.K. and A.I. performed the experiments and analysed the experimental data. E.M., R.V. and S.G. developed the supporting theoretical models. S.K., E.M., A.I., C.S. and J.F.W. performed the numerical studies for benchmarking the experimental data. I.B., M.A., S.G. and R.V. supervised the study. All authors contributed to the writing of the manuscript and to the discussion and interpretation of the results.

Funding

Open access funding provided by Max Planck Society.

Competing interests

The authors declare no competing interests.

Additional information

Supplementary information The online version contains supplementary material available at https://doi.org/10.1038/s41567-024-02611-z.

Correspondence and requests for materials should be addressed to Julian F. Wienand or Immanuel Bloch.

Peer review information *Nature Physics* thanks the anonymous reviewers for their contribution to the peer review of this work.